Optimization of parameters of chemical spray pyrolysis technique to get n and p-type layers of SnS

T.H. Sajeesh, Anita R. Warrier, C. Sudha Kartha, K.P. Vijayakumar *

Department of Physics, Cochin University of Science and Technology, Cochin-682 022, Kerala, India

ARTICLE INFO

ABSTRACT

SnS thin films were prepared using automated chemical spray pyrolysis (CSP) technique. Single-phase, p-type, stoichiometric, SnS films with direct band gap of 1.33 eV and having very high absorption coefficient ($>10^5$/cm) were deposited at substrate temperature of 375 °C. The role of substrate temperature in determining the optoelectronic and structural properties of SnS films was established and concentration ratios of anionic and cationic precursor solutions were optimized. n-type SnS samples were also prepared using CSP technique at the same substrate temperature of 375 °C, which facilitates sequential deposition of SnS homojunction. A comprehensive analysis of both types of films was done using x-ray diffraction, energy dispersive x-ray analysis, scanning electron microscopy, atomic force microscopy, optical absorption and electrical measurements. Deposition temperatures required for growth of other binary sulfide phases of tin such as SnS_2, Sn_2S_3 were also determined.

1. Introduction

In terms of cost and efficiency, thin film solar cells hold an optimistic fervor as future resource for sustainable energy. Now the most developed thin film photovoltaic technologies are based on CdTe and CuInSe₂ absorber layers. Recently a maximum efficiency of 19.9% has been achieved at National Renewable Energy Laboratory, United States of America, using Cu(In,Ga)Se₂ based absorber layers [1]. But these materials, due to the difficulty in maintaining stoichiometry, especially in large area films, alleged environmental hazards and high cost of indium are not beneficial in the longer run [2]. Hence there is an urgent need for the development of materials that are easy to prepare, eco-friendly and having easily available constituents. Tin (II) sulfide (SnS) is one such material, which has high potential in device fabrication due to its non-toxicity and easy availability of the constituent materials. It is a IV–VI layered compound semiconductor with distorted NaCl type orthorhombic crystal structure [3]. Due to its interesting structural, optical and electrical properties, SnS has become an important material for optoelectronics and photovoltaics [4–7] with many promising technological applications [8,9]. Further, properties like high absorption coefficient [10], direct band gap in the range 1.2–1.5 eV and indirect band gap in the range 1.0–1.2 eV [7,11] make SnS a more viable material for photovoltaic applications. Loferski theoretically proved that a maximum efficiency of 25% is achievable for this material [12]. Electronic structure and structural calculations of SnS were deduced from photoelectron spectra by Ettema et al. [13]. Opto-electronic properties suitable for the device fabrication were also reported by several groups [3–7].

SnS thin films could be prepared using different techniques such as vacuum evaporation [14], radio frequency sputtering [15], electrochemical deposition [16,17], atmospheric pressure chemical vapor deposition [18], plasma enhanced chemical vapor deposition [19], brush plating [20], dip deposition [21], chemical bath deposition [22] and chemical spray pyrolysis (CSP) [23]. Among these, CSP is one of the simplest and cost effective means of thin film deposition, especially when large area deposition is required. Moreover, the ease of doping and flexibility of tailoring the stoichiometry make this technique more popular in the field and adapt well to our requirements of photovoltaic device fabrication. Hence this technique was selected for the deposition of SnS thin films, in the present work.

2. Experimental details

Films were deposited using the indigenously designed and fabricated microprocessor controlled automated spray coating unit [24]. It consists of a base plate, in which a heater coil is embedded to facilitate heating, upon which the substrates for film deposition are to be placed. Substrate temperature (T_S) was maintained with the help of a feedback circuit which controls the heater supply. Temperature of the substrate can be varied from room temperature to 600 °C. During the spray, temperature of the substrate was kept constant with an accuracy of ± 5 °C. Spray head and heater with substrates were kept inside a chamber provided with an exhaust fan for removing gaseous by-

* Corresponding author.
E-mail address: kpv@cusat.ac.in (K.P. Vijayakumar).

products and vapors of the solvent. Pressure of the carrier gas can be adjusted manually. With the help of indigenously developed dispensing unit, the spray rate of the solution can also be precisely controlled. Spray rate is an important parameter in controlling different properties of the films and in the automated spray unit, this can be controlled so as to get good repeatability of film properties. The $X–Y$ movement of spray head can also be controlled using the microprocessor.

In the present work, precursor solutions were mixtures of doubly hydrated stannous chloride ($SnCl_2 \cdot 2H_2O$) and thiourea ($CS(NH_2)_2$). The usage of $SnCl_2$ instead of $SnCl_4$ reduces material cost as well as deposition temperature required for the deposition substantially, which is very vital for device level applications [25].

Cleaned soda–lime glass slides, with dimensions of $37 \times 12 \times 1.2$ mm^3 were used as the substrates. Clear aqueous solution of $SnCl_2 \cdot 2 H_2O$ and $CS(NH_2)_2$ were used as the starting anionic and cationic precursors respectively. For the present study, we prepared three sets of films namely 'Set A', 'Set B' and 'Set C'. For all the sets, distance of spray head from the substrate was 18 cm and total volume of the solution sprayed was 30 ml, which contained equal volumes (15 ml) of $SnCl_2 \cdot 2 H_2O$ and $CS(NH_2)_2$. The spray rate was fixed at 2 ml/min since low spray rate favored formation of films with superior surface morphology [24]. Further lowering of deposition rate would require longer coating durations, which is an undesirable condition. 'Set A' was prepared by varying T_S from 100 °C to 500 °C with an accuracy of ± 5 °C while the 'molarity of $SnCl_2 \cdot 2H_2O$' (M_{Sn}) and 'molarity of $CS(NH_2)_2$' (M_S) were kept constant at 0.1 M and 0.2 M respectively. We chose higher value for M_S considering the high vapor pressure of sulfur. After optimizing T_S, 'Set B' was prepared by varying M_S alone from 0.1 M to 0.4 M, keeping M_{Sn} fixed at 0.1 M, in order to optimize the composition ratio required for deposition of p-type SnS thin films. The third batch of samples, 'Set C' was prepared for developing n-type SnS. For that, M_{Sn} alone was varied from 0.06 M to 0.12 M, fixing M_S at 0.10 M. For 'Set B' and 'Set C' the T_S was fixed at 375 °C.

Thickness of the films was measured using Stylus method (Dektak 6 M thickness profiler). Structural analysis was performed employing x-ray diffraction (XRD) using Rigaku (D.Max.C) x-ray diffractometer having CuKα ($\lambda = 1.5405$ A °) radiation and Ni filter operated at 30 kV and 20 mA. All samples were scanned in the range 10° to 60° with a scan speed of 5°/min. Surface studies of the samples were done with the help of atomic force microscopy (AFM) (Nanoscope-E, Digital Instruments, USA, in contact mode) and scanning electron microscopy (SEM) (JEOL, JSM-840). Operating voltage for SEM measurements was 20 kV and the surface morphology of the samples was compared at 25,000× magnification. Compositional variation of the samples was analyzed using energy dispersive x-ray (EDAX) analysis (operated at 20 kV), which is attached with the SEM (JEOL JSM-840). Optical absorption studies were carried out using UV–Vis–NIR (190–2500 nm) spectrophotometer (Jasco V-750 model). Employing Keithley 236 source measure unit, electrical characterization and photosensitivity measurements were performed by applying an electric field of 1000 V/m to the films. Silver electrodes were painted on the surface of the film on a fixed area with uniform thickness, keeping a distance of 5 mm in between the electrodes for electrical characterizations. For photosensitivity measurements, the samples were illuminated with a tungsten halogen lamp (white light) capable of giving intensity of 60 mW/cm^2 over the sample surface. IR filter and a water column were kept in between the light source and sample to avoid heating of the sample.

3. Results and discussions

3.1. Optimization of substrate temperature

When T_S was in the range 300 °C to 400 °C, all the films were uniform, free of pinholes and crack, and having brownish gray color. These films had predominant SnS phase, crystallized in Herzenbergate orthorhombic structure, as observed from the XRD pattern (Fig. 1).
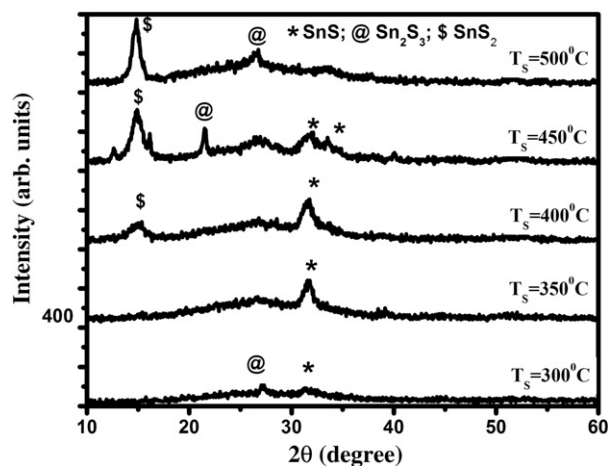

Fig. 1. XRD pattern of Sn$_x$S$_y$ films prepared at (a) $T_S = 300$ °C, (b) $T_S = 350$ °C, (c) $T_S = 400$ °C, (d) $T_S = 450$ °C and (e) $T_S = 500$ °C.

For $T_S < 250$ °C, white spots were observed all over the film surface, which indicated the presence of unreacted precursors, as T_S was lower than the "pyrolytic temperature". For $T_S > 450$ °C the films were yellowish in color with prominent SnS$_2$ phase. Fig. 1 shows XRD patterns of films deposited at different T_S (250 °C–500 °C) with SnS peak orientation along (111) plane having lattice parameters $a = 4.329$ Å, $b = 11.19$ Å, $c = 3.983$ Å, at $2\theta = 31.53°$ (JCPDS data card 39-0354). The XRD pattern clearly indicated prominent peaks of Sn$_2$S$_3$ phase at lower T_S (<300 °C) and SnS$_2$ phase at higher T_S (>400 °C). These impurity phases almost vanished for 350 °C$< T_S <$400 °C, and at 375 °C, the films were having better crystallinity with a nearly single-phase SnS (Fig. 2).

Grain size of the films was calculated from the peak at $2\theta = 31.53°$ using the Debye–Scherer formula, $D = 0.9\lambda/(\beta \cos\theta)$, where D is the diameter of the crystallites forming the film, λ is the wavelength of CuK$_\alpha$ line, β is the full width at half maximum in radians and θ is the Bragg angle. Grain size decreased slightly (from 12 nm to 9 nm) as the T_S increased from 300 °C to 400 °C. Grain size of the film prepared at $T_S = 375$ °C was 10 nm.

Surface morphology of the sample showed noticeable changes when T_S was increased from 300 °C to 375 °C. It is evident from the SEM image shown in Fig. 3a that the samples prepared at $T_S = 375$ °C had needle like polycrystalline growth, while from Fig. 3b, it is clear that for samples prepared at $T_S = 300$ °C the surface is smooth with regular spherical grains. Fig. 4a and b shows the AFM images of the samples prepared at $T_S = 300$ °C and $T_S = 375$ °C respectively. These images agreed well with the SEM images (Fig. 3a and 3b) and confirm
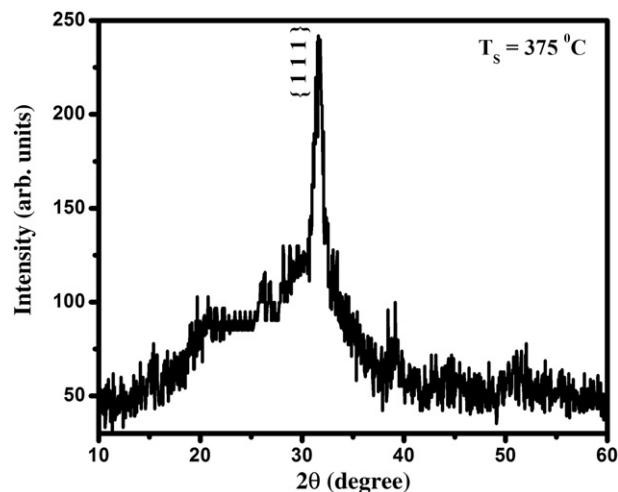

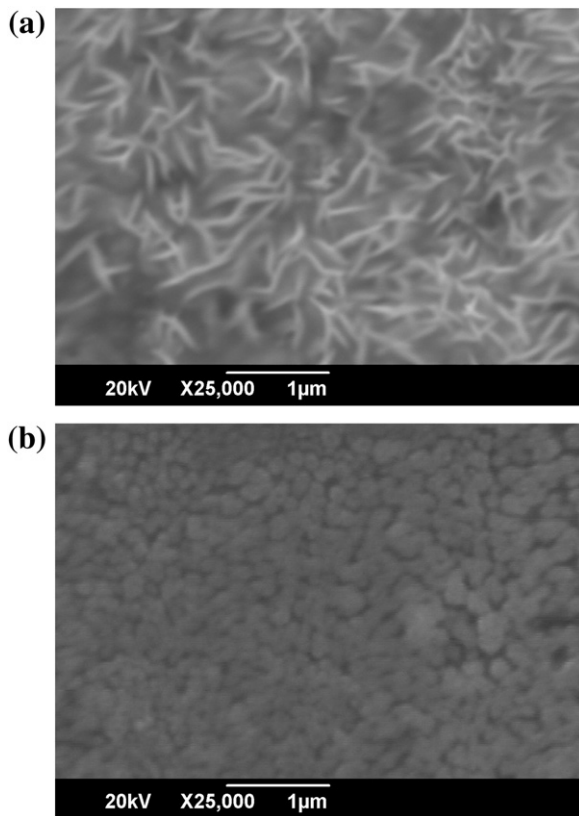Fig. 2. XRD pattern of SnS films prepared at $T_S = 375$ °C.

(a)

(b)

Fig. 3. SEM image of SnS films prepared at (a) $T_S = 375$ °C and (b) $T_S = 300$ °C.

that film surface changed from regular spherical grain structure to needle like structures with increase in temperature from 300 °C to 375 °C.

Thickness of the films decreased from 1.4 µm to 0.55 µm with the increase in T_S (Fig. 5). This might be due to the re-evaporation of the compounds at elevated temperatures. Such a decrease in thickness with increase in T_S for films fabricated using CSP has been reported earlier [26].

Atomic ratios of Sn and S in the films were examined using EDAX. Variation of Sn/S ratio in the films with respect to the T_S is depicted in Fig. 6. It was observed that, as T_S was increased, the sulfur incorporation in the film also increased, and at $T_S = 375$ °C we obtained nearly stoichiometric SnS films. But at still higher T_S (>400 °C) the sulfur content in the film started decreasing, probably due to re-evaporation of sulfur owing to its high vapor pressure.

Optical band gap of the films was determined from the $(\alpha h\nu)^2$ versus $h\nu$ plot (Fig. 7). All the samples had very high absorption coefficient (>10^5 cm^{-1}). Linearity of the graphs confirmed that all the Sn_xS_y thin films had direct band gap. Band gap of the SnS films prepared at $T_S = 375$ °C was 1.33 eV which is almost same as that for single-phase SnS films. For SnS films deposited in the range 350 °C<T_S<400 °C, band gap was found to vary. There was no significant variation in the grain size with T_S, in this temperature range which might affect the band gap. Fig. 8 depicts the variation of band gap for the entire range of T_S. Here we can observe close similarity with the graph giving the variation of Sn/S ratio (Fig. 6). This indicates the dependence of band gap on composition. The high value of band gap at lower and higher temperature is probably due to the formation of Sn_2S_3 and SnS_2 phases respectively [27].

Resistivity of the films decreased from 5×10^3 Ω cm to 5 Ω cm with the increase in T_S. High value of resistivity of the films prepared below 300 °C was probably due to presence of mixed valent compound Sn_2S_3. Hot probe analysis was carried out on the sample to determine the conductivity type. This measurement indicated that the films prepared in the range $T_S = 300$–400 °C were p-type and
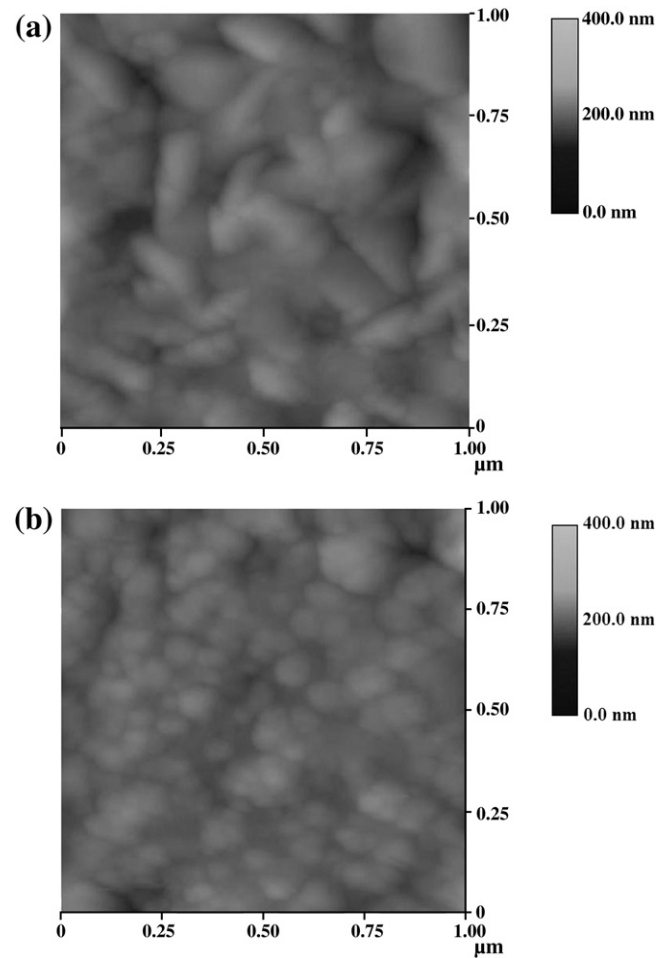
(a)

(b)

Fig. 4. AFM image of SnS films prepared at (a) $T_S = 375$ °C and (b) $T_S = 300$ °C.

those prepared at T_S>450 °C, (where the SnS_2 phase was dominating) were n-type. The films prepared at T_S<300 °C showed fluctuating nature in hot probe analysis, which may be due to the very high resistivity of these films. Hence it can be concluded that films prepared at 375 °C have the optimal qualities of an absorber layer in terms of crystallinity, high absorption coefficient, band gap and stoichiometry. Therefore $T_s = 375$ °C was chosen for further deposition of SnS films.
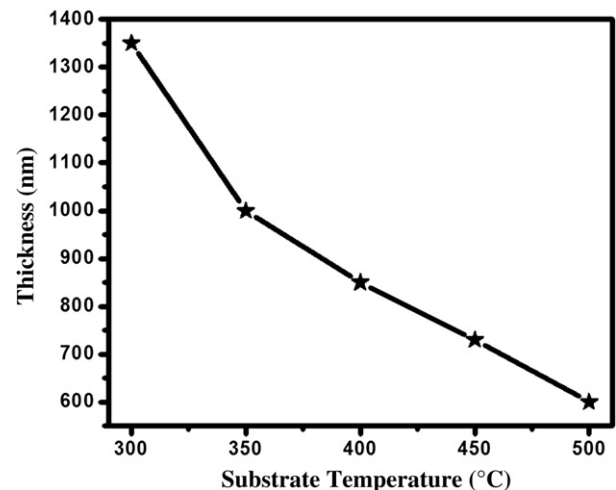

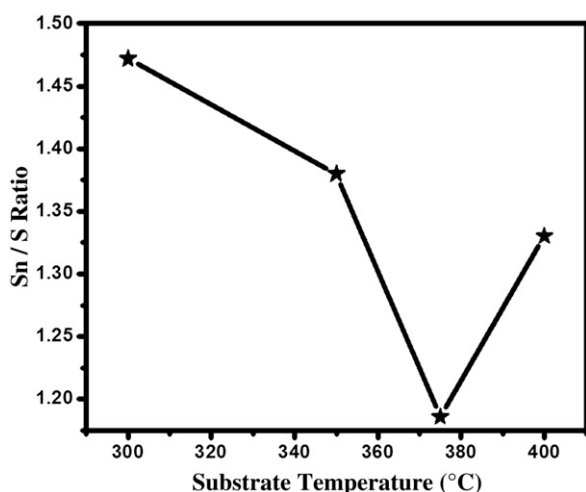**Fig. 5.** Variation of film thickness with T_S.

Fig. 6. Variation of Sn/S ratio in the film with T_S. Each point in the figure represents average of five experimental values obtained from different points of the sample.

Fig. 8. Variation of Bandgap of the films with T_S.

3.2. Optimization of precursor ratio for p-type SnS absorber layer

Ratio of anionic to cationic precursors in the spray solution plays a significant role in compound formation as well as in determining optoelectronic properties of the films, especially when the samples are prepared using CSP technique. Hence the 'Set B' films were prepared for optimizing concentration of precursors to obtain single-phase p-type SnS films so that it can be used as absorber layer in solar cells. Analyzing the films deposited by varying M_S, we could optimize M_S required for obtaining single-phase SnS at 375 °C. M_S of 0.2 M in the precursor solution resulted in the formation of films with SnS phase only. But for $M_S > 0.2$ M, SnS_2 was dominating and films with $M_S < 0.2$ M showed presence of the 'mixed valency' compound Sn_2S_3, as observed from the XRD pattern (Fig. 9). From these results it appears that, for a given ratio of precursors, there will be an optimum pyrolytic temperature, which favors formation of a particular compound and when we select 0.2 M as the value of M_S, the substrate temperature of 375 °C is found to be optimum for depositing SnS films.

Hot probe analysis indicated that SnS films thus deposited were p-type and resistivity measurements using 'two probe method' gave a resistivity value of 60 Ω cm.
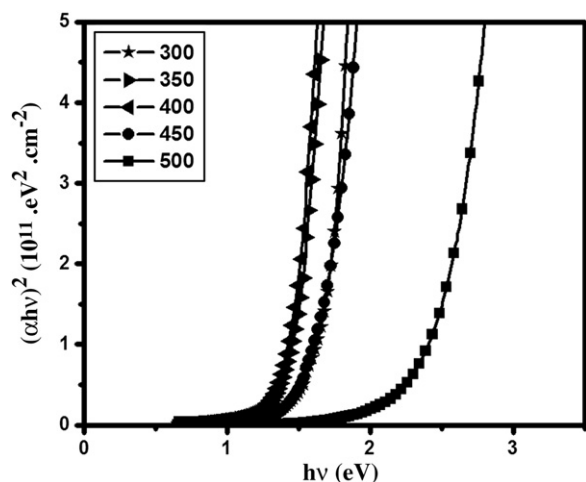
3.3. Deposition of n-type SnS film

Through the studies presented in the earlier sessions we could optimize conditions for obtaining p-type SnS films which could be used as the absorber layer. For deposition of the n-type SnS suitable for fabricating homojunction solar cells, 'Set C' was prepared by varying the metal concentration (M_{Sn}), since the conductivity type of the SnS films are essentially controlled by the Sn concentration in the compound. For fabrication of homojunction by sequential deposition employing CSP technique, it is beneficial to have the same T_S for both n and p-type layers. Hence we selected the previously optimized T_S (375 °C) for the preparation of 'Set C' also. For the present study, M_S was purposefully kept low since at higher M_S, the probability to grow Sn compounds with large Sn vacancies is high, resulting in the p-type films.

Hot probe analysis proved these samples to be n-type, only when M_{Sn} is 0.12 M. Further increase in M_{Sn} resulted in visibly non-uniform films. Fig. 10 shows the variation of resistivity of the samples with M_{Sn}. It was observed that resistivity decreases up to $M_{Sn} = 0.1$ M and then increased slightly for higher M_{Sn}. The slight increase in resistivity for $M_{Sn} = 0.12$ M could be due to type conversion.

Photosensitivity was measured using the formula, $G = \frac{I_L - I_D}{I_D}$, where G is the photosensitivity, I_D the dark current and I_L is the illuminated current measured under illumination. All the samples were illuminated for 1 min before recording I_L. Variation in photosensitivity was observed (Fig. 11) which followed the same trend as that of the resistivity (Fig. 10). A high photosensitivity of 2.3 was shown by films

Fig. 7. Plot of $(\alpha h\nu)^2$ versus $h\nu$ for the films prepared at (a) $T_S = 300$ °C, (b) $T_S = 350$ °C, (c) $T_S = 400$ °C, (d) $T_S = 450$ °C and (e) $T_S = 500$ °C.
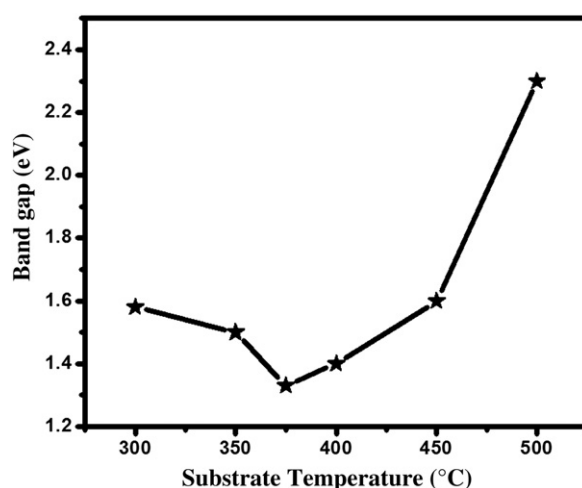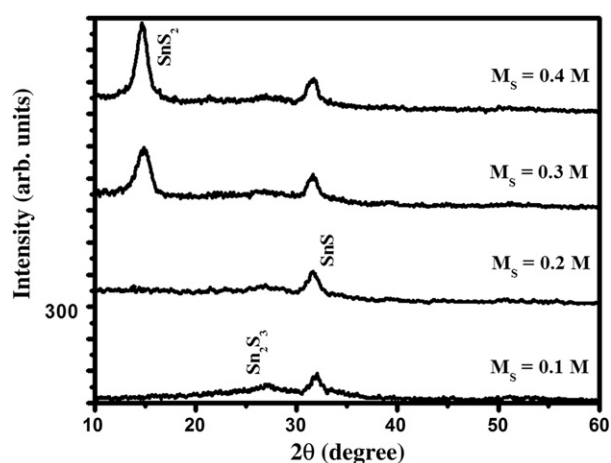

Fig. 9. XRD pattern of the sample prepared with (a) $M_S = 0.1$ M, (b) $M_S = 0.2$ M, (c) $M_S = 0.3$ M and (d) $M_S = 0.4$ M. For all the sets, M_{Sn} is kept constant at 0.1 M.
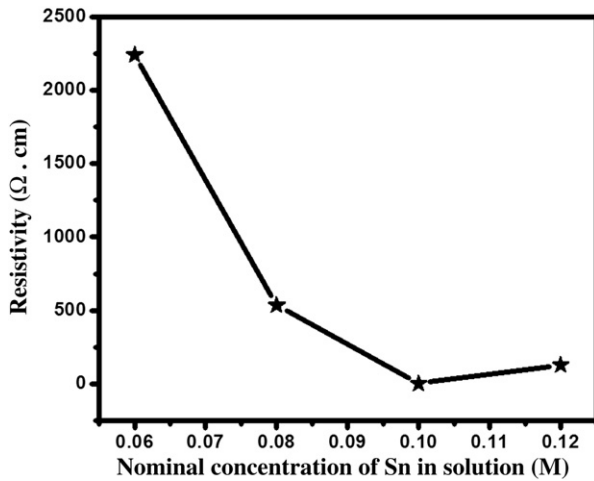
Fig. 10. Variation of resistivity with M_{Sn}.

Fig. 12. XRD pattern of the sample prepared with (a) $M_{Sn} = 0.06$ M, (b) $M_{Sn} = 0.08$ M, (c) $M_{Sn} = 0.10$ M and (d) $M_{Sn} = 0.12$ M. For all the sets, M_S is kept constant at 0.1 M.

prepared with $M_{Sn} = 0.06$ M. We could thus engineer the photosensitivity of SnS films by varying the concentration of Sn in spray solution.

Fig. 12 shows the XRD patterns of the samples prepared by varying M_{Sn}. These samples had Herzenbergate orthorhombic SnS phase with preferential orientation along (111) plane and crystallinity of the samples increased with the increase in M_{Sn}. The Sn_2S_3 impurity phase was present in all the samples irrespective of variation in M_{Sn} (Fig. 12). For higher M_{Sn} the films were metallic gray in color and their optical band gap decreased with increase in M_{Sn}. This increase in band gap could be attributed to the improvement in crystallinity with increase in M_{Sn}.

4. Conclusion

The deposition temperature and concentration of precursor solution were optimized for fabrication of stoichiometric SnS films that can be used as p-type, direct band gap absorber layer suitable for solar cells. Band gap engineering of single-phase SnS thin film was achieved in the temperature region 300 °C–400 °C, which finds application in fabrication of solar cells as here we need both lower and higher band gap layers. n-type SnS films could be obtained when content of the metal precursor is higher than that of the sulfur precursor in spray solution. As the deposition temperature is same for the deposition of both n and p-type SnS films, it is possible to have sequential deposition of n and p-type layers for fabrication of SnS homojunction. Highly photosensitive SnS
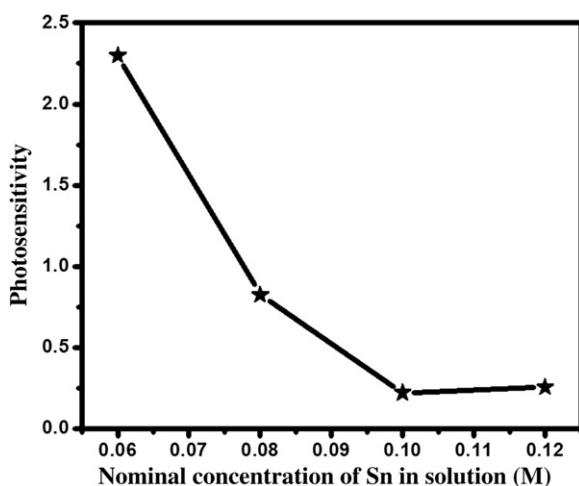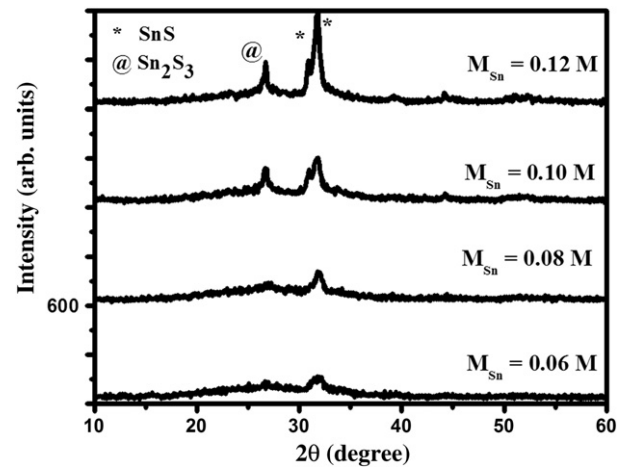
films which had photocurrent value thrice that of dark current, can also find application as smart material.

References

[1] J.I. Repins, M.A. Contreras, B. Egaas, C. De, Prog. Photovoltaics Res. Appl. 16 (2008) 235.
[2] T. Markvart, L. Castaner, Elsevier publication, New-York, 2003.
[3] W. Albers, C. Hass, H.J. Vink, J.D. Wasscher, J. Appl. Phys. 32 (1961) 2220.
[4] J.B. Johnson, H. Jones, B.S. Latham, J.D. Parker, R.D. Engelken, C. Barber, Semicond. Sci. Technol. 14 (1999) 501.
[5] P. Pramanik, P.K. Basu, S. Biswas, Thin Solid Films 150 (1987) 269.
[6] D. Avellaneda, G. Delgado, M.T.S. Nair, P.K. Nair, Thin Solid Films 515 (2007) 5771.
[7] G. Valiukonis, D.A. Guseinova, G. Keivaitb, A. Sileika, Phys. Status Solidi B 135 (1986) 299.
[8] T. Jiang, G.A. Ozin, A. Verma, R.L. Bedard, J. Mater. Chem. 8 (1998) 1649.
[9] A.T. Kana, T.G. Hibbert, M.F. Mahon, K.C. Molloy, I.P. Parkin, L.S. Price, Polyhedron 20 (2001) 2989.
[10] M. Parenteau, C. Carlone, Phys. Rev. B: Condens. Matter 41 (1990) 5227.
[11] H. Noguchi, A. Setiyadi, H. Tanamura, T. Nagatomoto, O. Omoto, Sol. Energy Mater. Sol. Cells 35 (1994) 325.
[12] J.J. Loferski, J. Appl. Phys. 27 (1956) 777.
[13] A.R.H.F. Ettema, R.A. de Groot, C. Hass, T.S. Turner, Phys. Rev. B: Condens. Matter 46 (1992) 7363.
[14] L. Price, I.P. Parkin, A.M.E. Hardy, R.J.H. Clark, Chem. Mater. 11 (1999) 1792.
[15] W.G. Pu, Z.Z. Lin, Z.W. Ming, G.X. Hong, C.W. Quin, Proceedings of the first world conference on Photovoltaic Energy Conversion, Hawaii, Dec 5–9 1994, p. 365.
[16] S. Cheng, Y. Chen, C. Huang, G. Chen, Thin Solid Films 500 (2006) 96.
[17] Z. Zainal, M.H. Sussein, A. Kassim, A. Ghazali, Sol. Energy Mater. Sol. Cells 40 (1996) 347.
[18] L.S. Price, I.P. Parkin, T.G. Hillbert, K.C. Molloy, Chem. Vapor. Depos. 4 (1998) 222.
[19] A.S. Juarez, A. Ortiz, Semicond. Sci. Technol. 17 (2002) 931.
[20] B. Subramanian, C. Sanjeeveiraja, M. Jayachandran, Sol. Energy Mater. Sol. Cells 79 (2003) 57.
[21] C.R. Sehhar, K.K. Malay, D.D. Gupta, Thin Solid Films 350 (1999) 72.
[22] P. Pramanik, P.K. Basu, S. Biswas, Thin Solid Films 150 (1987) 269.
[23] H. Ben Haj Salah, H. Bouzouita, B. Rezig, Thin Solid Films 480–481 (2005) 439.
[24] T. Sebastian, R. Jayakrishnan, C. Sudha Kartha, K.P. Vijayakumar, Open Surf. Sci. J. 1 (2009) 1.
[25] G. Gordillo, L.C. Moreno, W. de. La Cruz, P. Teheran, Thin Solid Films 252 (1994) 61.
[26] K.L. Chopra, S.R. Das, Plenum Press, New-York, 1983.
[27] N. Koteeswara Reddy, K.T. Ramakrishna Reddy, Physica. B 368 (2005) 25.

Fig. 11. Variation of photosensitivity with M_{Sn}.